Experimental and Numerical Analysis of Geometrical Properties of Laser Metal Deposited Titanium

Esther T. Akinlabi *IAENG MEMBER*, Mohammed A. Tayob and Francesco Pietra

Abstract**—**Laser metal deposition (LMD) is a manufacturing process, which can be used to manufacture a complete, fully functional part by building it up layer-by-layer using the data from a Computer-Aided-Design (CAD) file. The layer-by-layer addition can also be used to rebuild worn-out sections of existing parts, as well as to deposit protective coatings to protect parts in surface engineering. In order to produce parts with high geometrical tolerances and desirable material properties, the process parameters have to be carefully controlled. Since the LMD process requires the interaction of parameters, it is not always easy to predict the output geometry. In this paper, the laser metal deposition process was modelled in ANSYS Parametric-Design-Language (APDL), using a transient thermal analysis, in order to determine the geometrical properties of the clad, that is, the width and the height of the resulting clad. The simulated results were then compared experimentally by depositing Commercially Pure (CP) titanium powder onto a Ti-6Al-4V substrate, in order to verify the simulation. The varying parameter in the experimental process was the powder flow rate, which was varied between 0.5-2.5g/min. In addition to the geometrical properties, the microstructure, microhardness; and the porosity levels of the deposited clads were also analyzed, in order to better determine the clad quality and integrity. The model showed good agreement in predicting both the height and the width of the clads. Porosity was noticed in all the samples with the exception of the clad deposited at the lowest powder flow rate setting of 0.5 g/min. An increase in the powder flow rate also led to a smaller fusion zone, due to a lower laser-material interaction period, which was the result of the increase in the quantity of powder causing attenuation of the beam, and less laser power being absorbed by the substrate.

Keywords**—** *ANSYS, Heat-Affected Zone, laser metal deposition, microhardness, microstructure, porosity, powder flow rate, titanium.*

Manuscript revised on March 25 2016

Esther T. Akinlabi is an Associate Professor and the Head of Department of the Department of Mechanical Engineering Science, Auckland Park Kingsway Campus, University of Johannesburg, Johannesburg, South Africa, 2006. (E-mail: etakinlabi@uj.ac.za)

Mohammed A. Tayob is a Graduate Candidate in the Department of Mechanical Engineering Science, Auckland Park Kingsway Campus, University of Johannesburg, Johannesburg, South Africa, 2006. (E-mail: maq.tayob@gmail.com).

Francesco Pietra is a Senior Lecturer in the Department of Mechanical and Aeronautical Engineering, University of Pretoria, South Africa. (Email: Pietra.Francesco@up.ac.za)

I. INTRODUCTION

The modern manufacturing era has called for a reduction in manufacturing costs; yet at the same time, it requires constant development of components. Traditional machining, especially in the case of small complex components is time consuming and expensive. Additive manufacturing methods such as Laser Metal Deposition (LMD) have therefore found favor in recent times as it allows small complex components to be developed at a much faster and cheaper rate compared to traditional manufacturing methods [1]. This is especially true in the case of titanium which is classified as a difficult-to-machine material. LMD is an additive manufacturing method that works by irradiating the surface of a substrate material, using a high-power laser beam, which is shielded by an inert gas to prevent oxidation, to form a melt pool on the substrate material, into which a powder is fed [2] [3] [4]. The powder is partially melted by passing through the laser; and it also melts, along with a portion of the base material, thereby forming a metallurgical bonded layer similar to a weld, but with a higher mechanical strength and improved material properties. The layer-by-layer addition of material is extremely versatile and can not only be used to build complete components but can also be used to rebuild damaged or worn out sections allowing LMD to be used as a repair process as well [1]. A schematic of the LMD process can be seen in Figure 1.

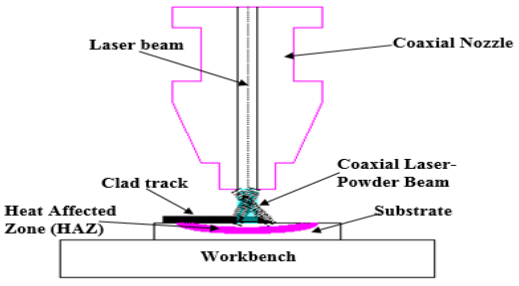

Fig. 1: Schematic of the LMD process

As with all techniques, constant research is being done to improve the process. Due to the complex inter-relationships that exist between the processing parameters, it is often difficult to successfully predict the geometrical properties of the clad. Therefore, researchers have attempted to simulate the LMD process in order to better predict the geometry.

ISBN: 978-988-14048-0-0
ISSN: 2078-0958 (Print); ISSN: 2078-0966 (Online)

Numerous approaches have been taken. Some researchers have developed analytical models; some have developed numerical models, and some have used a combination of both analytical and numerical techniques. Lalas *et al* [5] developed an analytical model to determine the clad geometry. The model took into account the scanning speed and the powder flow rate. The model works in two steps: the first step assumes that the clad is liquid and that the substrate is solid; while the second step assumes that both the clad and substrate are liquid. The assumption used to determine the clad characteristics was based on the phenomenon of surface tension. The model was shown to be capable of predicting clad accuracy with reasonable accuracy at medium to low-to-medium process speeds. Cheikh *et al* [6] had noticed that the cross-sectional geometry of the clad forms a disk shape – due to surface tension forces. Therefore, if one could determine the shape of the disk, one could effectively determine the shape of the clad. This observation was used to develop an analytical relationship between the radius and the centre of the disk, on the one hand, and the process parameters, on the other hand. The circle centre position and the radius were related to the powder efficiency and width; where the width could be obtained, either by using a parametric relationship, or by using a thermal analytical relationship; while the powder efficiency could only be obtained parametrically. The model was shown to be able to predict the geometry with a reasonable degree of certainty. Peyre *et al.* [7] developed an analytical and numerical model of the LMD process. The model only considered experimental parameters, such as the powder flow rate, laser power and scanning speed as input data. The main assumption of the model is that the powder flow rate contributes to clad formation, provided that the incoming powder interacts with the molten pool, and that the energy inside the melt pool is high enough to melt the powder. The melt-pool geometry, which is also the clad width, is calculated by using steady-state finite element calculations; while the height was calculated analytically. The model was shown to reproduce experiments rather well. Fallah *et al.* [8] developed a transient finite element approach to simulate the clad geometry. The model did not require any assumptions of the general shape to determine the clad geometry. The addition of powder was numerically carried out in a coupled manner by activating a new set of elements within each time step. The model was shown to be highly accurate in determining the clad geometry.

In this study the LMD process was modelled in ANSYS APDL using a transient thermal analysis in order to determine the geometrical properties of a single layer clad. To validate the model outputs produced by the simulation CP titanium was deposited onto a Ti-6Al-4V substrate and the geometry was measured macroscopically. In order to determine the integrity of the clads produced during the LMD process, further experimental work was performed to evaluate the effect of the parameters on the microstructure, microhardness and porosity levels in the clads.

II. Experimental Setup

The LMD process was conducted using a 4.4.kW RofinSinar™ Nd:YAG laser and a powder feeder with a coaxial nozzle powder, which was aligned to be concentric to the laser beam. The laser and deposition head were carried by a KUKA robot that controls the deposition process. The samples produced were 5 single clad passes of commercially pure titanium all deposited on the same Ti-6Al-4V titanium alloy substrate 5 mm apart, each with a track length of 80 mm. Argon was used as both the powder-delivery gas and as a shielding gas.

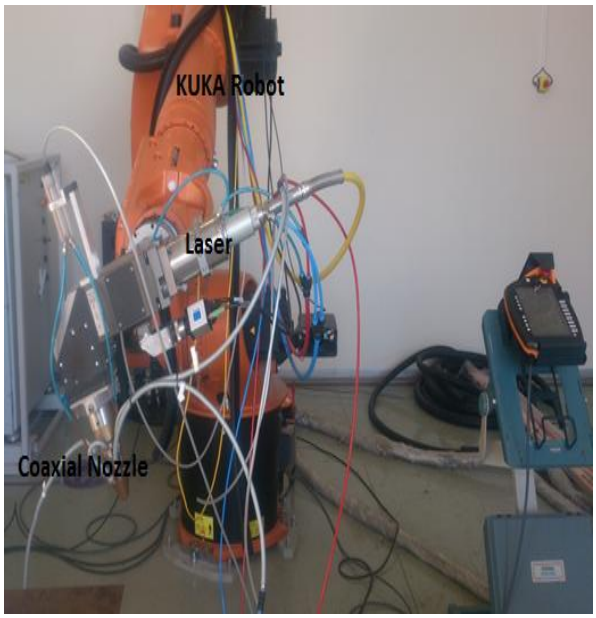

Fig. 2: Experimental Setup

The substrate on which the CP titanium was deposited was a grade 5 Ti-6Al-4V titanium alloy block with dimensions of 120 x 120 x 8 mm^3. The substrate was prepared by cleaning dirt and grime using sandblasting. The substrate was then washed with acetone to remove any residual sandblasted material that remained on the surface and air dried. The samples were produced by varying the powder flow rate from 0.5 g/s to 2.5 g/s in steps of 0.5 while keeping all other processing parameters constant, viz; the laser power at 1000 W, the beam diameter at 4 mm, the gas flow rate at 2 l/min and the scanning speed at 2 mm/s. The samples produced were then cut and prepared metallurgically, according to ASTM E3 – 11, standard guide for the preparation of metallographic specimens. The samples were then etched with Kroll's reagent. Scanning Electron Microscopy (SEM) (Tescan VEGA3) was used to characterize the microstructure and porosity of the samples. An EMCOTEST DuraScan microhardness tester was used to perform the microhardness tests in according to ASTM E384-11 standards. The average microhardness was determined by taking the average value of the indentations taken along the centre of the cross-sectional area of the clad from top to bottom.

III. Description of the Model

A. Mathematical representation

In order to determine the 3D time-dependent temperature distribution throughout the substrate and the clad, the transient heat-conduction equation must be solved. The

ISBN: 978-988-14048-0-0
ISSN: 2078-0958 (Print); ISSN: 2078-0966 (Online)

equation is represented by the formula below [9] [10] [11] [12]:

$$\frac{\partial}{\partial x}\left(k\frac{\partial T}{\partial x}\right)+\frac{\partial}{\partial y}\left(k\frac{\partial T}{\partial y}\right)+\frac{\partial}{\partial z}\left(k\frac{\partial T}{\partial z}\right)+Q=\frac{\partial(\rho C_p T)}{\partial t}$$ ……equation 1

Where k is thermal conductivity (W/mK), Q is Power generated per unit volume (W/m^3), ρ is density (kg/m^3), C_p is Specific heat Capacity (J/kg.K) and T is Temperature (K).

The solution can be obtained by substituting the appropriate initial and boundary conditions. The initial condition is that when the process has not started (t=0), the temperature is assumed to be at room temperature. For x,y, and z, this can be mathematically represented as:

Initial conditions for the substrate;

$$T(x,y,z,0)=T_0$$

Initial conditions for the newly added material in each solution time step [8] [10] [11] [12]:

$$T(x,y,z,t_{activation})=T_0$$

For both the substrate and the activated material:

$$T(x,y,z,\infty)=T_0$$

The convection and radiation boundary conditions are applied to all the outer surfaces:

$$K(\nabla T.\boldsymbol{n})=[-h(T-T_0)-\epsilon_r\sigma_r(T^4-(T)^4)]$$

The effect of the moving laser can be added into the boundary conditions; and therefore, the area of the substrate under the laser beam irradiation can be defined as [8] [10] [12]:

$$K(\nabla T.\boldsymbol{n})=[-\beta I-h(T-T_0)-\epsilon_r\sigma_r(T^4-(T)^4)]$$

Where T_0 is the ambient temperature (K), $t_{activation}$ is the time of addition of deposited material into the system, **n** = normal vector of the surface, I is the laser-power distribution on the substrate (W/m^2), σ_r is the Stefan-Boltzmann constant = 5.670 x 10^{-8} W/m^2 K^4, h is the heat convection coefficient (W/m^{2}K), T is the Temperature (K) and ε_r is the emissivity

B. Assumptions and Adjustments

(1) The laser-power intensity distribution is defined as a circular Gaussian TEM_{00} mode [8]:

$$I(r)=\frac{2P}{\pi r_L^2}exp\left(\frac{-2r^2}{r_L^2}\right)$$

Where I is the laser power intensity (W/m^2), P is the laser power (W), r_L is laser beam radius (m) and r is the distance from the centre of the laser beam (m).

(2) Absorption rate is only varied between 30-50%. [13]

(3) The base and track are assumed to be isotropic.
(4) The laser moves with a constant velocity.
(5) The evaporation of material is not taken into consideration.
(6) Material properties are independent of temperature (linear-material model)
(7) The effect of latent heat of is fusion ignored.
(8) The thermal conductivity value was multiplied by a factor of 2.5 for temperatures higher than the melting temperature to take into account the effect of Marangoni flow.
(9) The heat convection coefficient is taken as 40W/m2K for all temperatures.
(10) The powder-catchment efficiency is taken to be 50%.

C. Solution Strategy

The simulation process begins by deactivating the track elements and solving the heat transfer equations for the irradiated substrate, which is at room temperature. The temperature distribution in the material will therefore be obtained and the melt-pool boundary can be approximated based on the melting temperature of the powder material. Within the melt-pool boundary; wherever the temperature of the material exceeds the melting temperature of the powder material, a set of elements will be activated to form the track and it is based on the height of the deposited particles which is calculated using the following term [8]:

$$\Delta h=\frac{\dot{m}C\Delta t}{\rho_p(\pi r_{L^2}+2r_L V\Delta t)}$$

Where Δt= the solution-time step (s), m is the powder flow rate (kg/s), ρ_p is powder density (kg/m^3), V is the laser-scan velocity (m/s) and r_L is the laser radius (m).

IV. RESULTS AND DISCUSSION

A. Geometrical evaluation

The height, width, fusion zone and heat-affected zone were measured macroscopically. The measurements of the deposited zones are presented in Figure 3 and is summarized in Table 1.

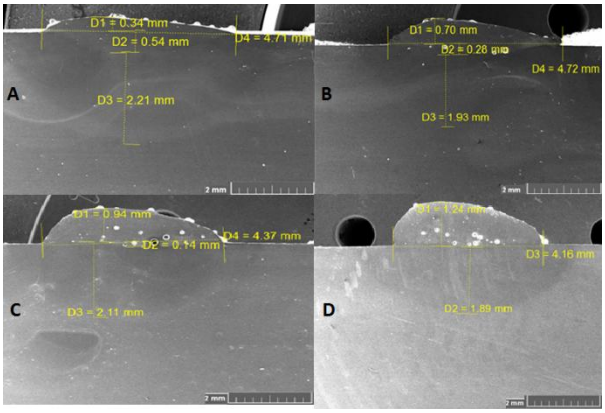

Fig. 3: Geometrical measurements of LMD produced clads

ISBN: 978-988-14048-0-0
ISSN: 2078-0958 (Print); ISSN: 2078-0966 (Online)

TABLE 1
GEOMETRICAL MEASUREMENTS

Sample	Width (mm)	Height (mm)	Fusion zone (mm)	HAZ (mm)
1	4.71	0.34	0.54	2.21
2	4.72	0.70	0.28	1.93
3	4.37	0.94	0.14	2.11
4	4.16	1.24	-	1.89
5	-	-	-	-

It was observed that as the powder flow rate increased, the width of the clads decreased, while the height increased. A good understanding of this phenomenon is related to the laser-material interaction during the LMD process. The un-melted powder particles first pass through the laser beam before landing in the melt-zone [14] [15]. This causes the powder to melt before reaching the melt-pool; but it attenuates some of the laser power, which means that less power is available to melt the substrate. Due to the less power being available to the substrate, a narrower melt-pool is created, which means that naturally the width of the clad would also be narrower. Effectively by increasing the powder flow rate, it has the same effect as decreasing the laser power to the substrate. The height, however, continues to increase; because there is sufficient energy to melt the incoming powder particles on the substrate. In order to confirm why the width was decreasing – due to less power input to the substrate to cause melting, it would be useful to have a look at the fusion zone. The fusion zone, as expected, decreases with an increase in the powder flow rate. It reaches a point where there is actually no fusion zone; and the clad is being deposited on the substrate without forming a proper bond or fusing to the substrate. Sample 4, produced at a powder flow rate setting of 2.0 g/min, had no measurable fusion zone; but it managed to bond onto the substrate. Sample 5, produced at a powder flow rate setting of 2.5 g/min, also had no fusion zone, which led to a defective clad; as the clad fell off the substrate, and hence its properties could not be evaluated further. The fusion zone in sample one was more representative of an alloying process; whilst the remaining samples had a fusion zone that was more representative of the cladding process.

The heat from the laser penetrated quite deep into the substrate; and, although not very clearly defined, the measured heat-affected-zones (HAZs) were similar, and ranged between 1.89-2.21mm between the samples, which is a range difference of less than 17%.

B. Microstructures of the deposited zone

In order to determine the effect of the LMD process on the microstructure of CP titanium, the cladded layers were analyzed. The micrographs of the cladded layers were taken in the deposit zone (positive bead area) from around the centre of the clad.

The micrographs of the cladded zone of the samples are presented in Figure 4. The LMD process requires both the substrate and the metal powder to melt, which means that it has to be heated to over 1400°C for the process to occur, which is above the 882°C transition temperature from a hexagonal-close-packed (HCP) structure to a body-centred cubic (BCC) structure; and then typical of the LMD process, it has a rapid cooling rate. When titanium is heated above the transition temperature and cooled rapidly from above 900°C, it forms hexagonal alpha martensite.

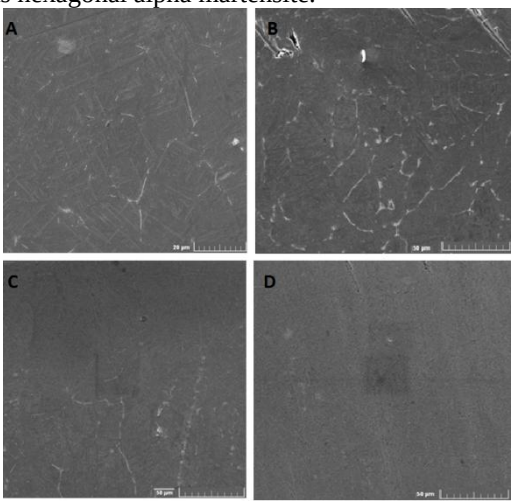

Fig. 4: Micrographs of clad zones. A) 0.5g/s B)1.0g/s C)1.5g/s D)2.0g/s

The microstructure in the clad zone was consistent for all the samples, which is an acicular alpha martensite microstructure, which is also commonly referred to as the alpha-prime microstructure. This consists of an alpha phase microstructure with a thin needle-like microstructure as expected and earlier reported in the literature [15].

C. Microhardness profiling

The average hardness of the clad layer for all the samples produced is presented in Figure 5.

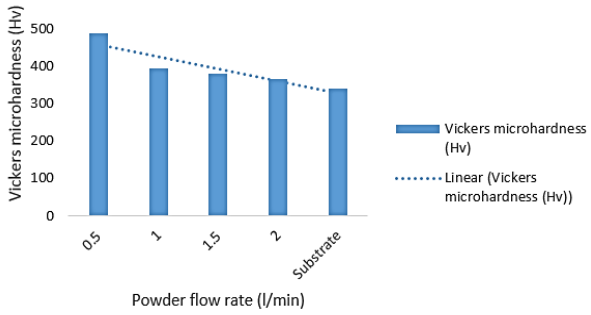

Fig. 5: Average Vickers microhardness of clads and substrate

The average microhardness of the clad zone starts out quite high on the sample produced at a low powder flow rate of 0.5 g/min; but it decreases, as the powder flow rate increases. With reference to the fusion zone, a correlation between microhardness and the size of the fusion zone was observed. As the fusion zone decreases, the microhardness also starts to decrease. In order to explain this phenomenon, it should be noted that commercially pure (CP) titanium, in sintered form, has a microhardness value of around 200HV; whereas Ti6-Al-4V in sintered form has a microhardness of approximately 350 [16]. Therefore, when the fusion zone is high, it means that the clad formed is actually an alloy of CP

ISBN: 978-988-14048-0-0
ISSN: 2078-0958 (Print); ISSN: 2078-0966 (Online)

titanium and Ti-6Al-4V (due to the thermo-capillary flow causing them to mix).

The microhardness of an alloy of Ti-6Al-4V and CP titanium would naturally be higher than the microhardness of just CP titanium. It is important to note that the microhardness for the samples is higher than both CP titanium and Ti-6Al-4V in ordinary form – that is not heat-treated [17] [18]. Sample 4 (flow rate of 2.0 g/min) is basically a clad consisting of only CP titanium; and it has a microhardness value of almost double that of sintered CP titanium, which illustrates the effect of the laser on microhardness. The microhardness of the HAZ is not significantly higher than that of the average microhardness of the substrate – with only an increase of around 15% higher compared to the substrate material. This highlights the significance of the LMD process compared to other processes; as the HAZ is very controlled.

D.Defect Characterization

With the exception of sample one, the lowest powder flow rate, all of the samples contained porosity. Porosity could form because of the unmelted powder particles, or as a result of gas entrapment. The spherical or blow-hole kind of shape of the porosity, which is shown in Figure 6 (B, C and D), is indicative of gas porosity.

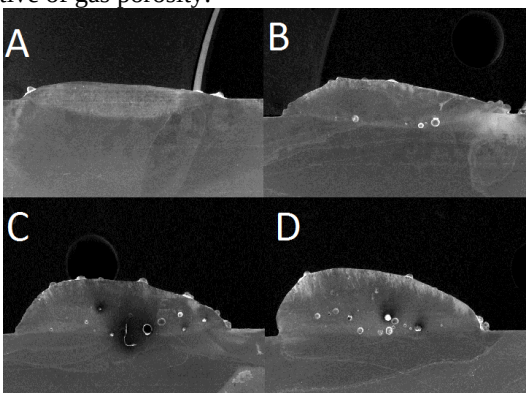

Fig. 6: Porosity in samples A)0.5g/s B)1.0g/s C)1.5g/s D)2.0g/s

Gas porosity can originate from a few sources. The gas could come from gas trapped in the powder feeders, it could be released from the powder particles themselves or it could be picked up from the environment since the experimental setup is not completely shielded from the environment. The porosity is also affected by the turbulence in the melt pool [19] [20]. The higher the turbulence, the greater the chance of gases to merge together. In this case, it was noticed that the porosity was present in all the samples, except the first one. The first sample (A) differs in two noticeable aspects from the other samples, in that it had the lowest powder flow rate; and secondly, the clad height formed is also the lowest. This can be attributed to the fact that as the powder flow rate increases, there is less laser material interaction leading to porosity; and secondly, as the height of the clad increases, it also leads to the emergence of porosity. This could indicate two things: the first is that either the powder itself contributes to the porosity due to the fact that more powder is deposited because more gas is released from the powder [21]. The second is that the increase in height could mean that any gas entering the system, either from the powder itself or from the environment, could not escape fast enough because of the increase in the height, especially because the LMD has rapid solidification rates.

Although, porosity is desirable for biomedical applications, it is a limitation for structural applications [20]. However, both the increase in the powder flow rate and the height are directly caused by an increase in the powder flow rate; and therefore, an increase in the powder flow rate led to porosity.

E. Simulation Results and Model Verification

The simulation was verified by comparing the output height and width of the simulated LMD process to the actual clad height and width obtained during the actual deposition process. The optimum mesh size selected was a mesh size of 0.2mm as it gave good accuracy while allowing the simulation to run within a feasible timeframe. It should also be noted that the model used linear material properties; the material properties did not change with a change in temperature. The cross-section of the clads produced using the simulation are presented in Figure 7.

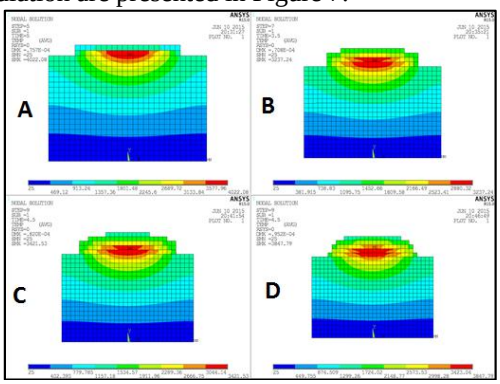

Fig. 7: Cross-section of clads obtained using simulation

The results of the simulated height are compared to the results of the actual height in Table 2.

TABLE 2
SIMULATED HEIGHT VS. ACTUAL HEIGHT

Powder flow rate (g/s)	Simulated height (mm)	Actual height (mm)	Difference (mm)	Error (%)
0.5	0.40	0.34	+0.06	+16.7
1.0	0.80	0.70	+0.10	+14.3
1.5	1.00	0.94	+0.06	+6.4
2.0	1.00	1.24	- 0.24	- 19.4

From Table 2, it was observed that at the lowest powder flow rate, there is a positive error of approximately 17%. This means that the model is building the height, more than it should. A logical explanation for the error is due to the lowest powder flow rate having the lowest height, coupled with a large element size, which means that it is the most vulnerable to errors. At a slightly higher powder flow rate, the actual difference is larger when compared to the lowest powder flow setting; but since it is not as sensitive, the error is reduced slightly. The simulated results at the powder flow rate setting of 1.5g/min showed the best results, with an error of only 6.4%. At the highest powder flow rate, the error

ISBN: 978-988-14048-0-0
ISSN: 2078-0958 (Print); ISSN: 2078-0966 (Online)

changes from a positive error to a negative error, which means that instead of overbuilding, the model is now underbuilding the geometry. A possible explanation for the underbuilding of the model is caused by using a linear material model, which does not take into consideration titanium's large increase in conductivity at temperatures higher than its melting temperature.

The comparison of the simulated width to the actual width is presented in Table 3.

TABLE 3
SIMULATED WIDTH VS. ACTUAL WIDTH

Powder flow rate (g/s)	Simulated width (mm)	Actual width (mm)	Difference (mm)	Error (%)
0.5	4.00	4.71	-0.71	-15.1
1.0	4.00	4.72	- 0.72	-15.3
1.5	4.40	4.37	-0.03	-0.7
2.0	4.40	4.16	+0.24	+5.8

Contrary to what happened with the height, the width showed a negative error for the powder flow rate settings of 0.5 -1.5g/min. However, at the powder flow rate setting of 1.5g/min, the model was able to simulate the width with an accuracy greater than 99%. At the highest powder flow rate, the simulated width was larger than the actual width by approximately 6%. Overall, the model was shown to simulate both the height and width with good accuracy. The model could determine both height and width with an accuracy of within 80% of the actual height and width; with accuracy increasing to over 90% in the case of the powder flow rate of 1.5g/min.

V. CONCLUSION

Using a transient finite-element approach, it was illustrated that it was possible to simulate the LMD process for varying powder flow rates with a high degree of accuracy. Additional experimental work revealed important information with regard to the clad quality. The first observation was that as the powder flow rate increased, it resulted in an increase in porosity and this can be attributed to more trapped gas being released from the gas atomized powder, as the powder flow rate increases, the increasing height reduces the chance of entrapped bubbles escaping or a combination of both factors. However, both factors are directly a consequence of an increase in the powder flow rate. The increase in the powder flow rate also had other detrimental effects; as it led to poor adhesion between the clad and the substrate. The results of this study form a basis to simulate clad geometries.

ACKNOWLEDGEMENT

The authors acknowledge the staff members of National Laser Centre that assisted with operating the machine and the University of Johannesburg Research Fund. Esther Akinlabi acknowledges the Johannesburg Institute of Advanced Study for the writing fellowship award (February to May, 2016) during when this manuscript was developed.

REFERENCES

[1] A. Angelastro, S. L. Campanelli, G. Casalino and A. D. Ludovico, "Analysis of a tool steel sample obtained by direct laser deposition," in *Annals of DAAAM for 2007 and Proceedings of the 18th International DAAAM symposium*, Zadar, Croatia, 2007.

[2] R. M. Mahamood, E. T. Akinlabi, M. Shukla and S. Pityana, "Laser Metal Deposition of Ti6Al4V: A study on the effects of Laser Power on Microstructure and Microhardness," in *International MultiConference of Engineers and Computer Scientists*, Hong Kong, 2013.

[3] F. W. Liou, "Direct Laser Deposition," in *Rapid Prototyping and Engineering Applications: A Toolbox for Prototype Development*, NW, USA, CRC Press, 2008, pp. 281-283.

[4] A. Kumar, C. P. Paul, A. K. Pathak, L. M. Bhargava and L. M. Kukreja, "A finer modeling approach for numerically predicting single track geometry in two dimensions during Laser Rapid Manufacturing," *Optics & Laser Technology*, vol. 44, pp. 555-565, 2012.

[5] C. Lalas, K. Tsirbas, K. Salonitis and G. Chryssolouris , "An analytical model of the laser clad geometry," *International Journal of Advanced Manufacturing Technology*, vol. 32, pp. 34-41, 2007.

[6] H. E. Cheikh, B. Courant, J. Y. Hascoet and R. Guillen, "Prediction and analytical description of the single laser track geometry in direct laser fabrication from process parameters and energy-balanced reasoning," *Journal of materials processing technology*, no. 212, pp. 1832-1839, 2012.

[7] P. Peyre, P. Aubry, R. Fabbro, R. Neveu and A. Longuet, "Analytical and Numerical modelling of the direct metal deposition laser process," *Journal of Physics D: Applied Physics*, vol. 41, pp. 1-10, 2008.

[8] V. Fallah, M. Alimardani, S. F. Corbin and A. Khajepour, "Temporal Development of melt-pool morphology and clad geometry in laser powder deposition," *Computational Materials Science*, vol. 50, pp. 2124-2134, 2011.

[9] T. Amine, J. W. Newkirk and F. Liou, "An investigation of the effect of Direct metal depostion parameters on the characteristics of the deposited layers," *Cases Studies in Thermal Engineering*, vol. 3, pp. 21-34, 2014.

[10] M. R. Frewin and D. A. Scott, "Finite Element Model of pulsed laser welding," Welding Research Supplement, NSW Australia, 1999.

[11] G. Zhu, A. Zhang, D. Li, Y. Tang, Z. Tong and Q. Lu, "Numerical simulation of thermal behaviour during laser direct metal deposition," *International Journal of Advanced Manufacturing technology*, vol. 55, pp. 945-954, 2011.

[12] Y. Li and D. Gu, "Thermal Behaviour during selective laser melting of commercially pure titanium powder: Numerical simulation and experimental study," *Additive Manufacturing*, vol. (Accepted manuscript) , no. http://dx.doi.org/10.1016/j.addma.2014.09.001, 2014.

[13] D. G. Mixon and W. P. Roach, "A thermal model for laser absorption," in *Conference on optical interactions with Tissue and cells*, San Jose, California, 2007.

[14] I. Tabernero, A. Lamikiz, S. Martinez, E. Ukar and L. N. Lopez de Lacalle, "Modelling of energy attenuation due to powder flow-laser beam interaction due to the cladding process," *Journal of materials processing technology*, vol. 212, pp. 516-522, 2012.

[15] J. Dong, F. Li and C. Wang, "Micromechanical behaviour study of alpha phase with different morphologies of Ti-6Al-4V alloy by micro indentation," *Material Science and Engineering A*, vol. 580, pp. 105-113, 2013.

[16] A. R. Hamad, J. H. Abboud, F. M. Shuaeib and K. Y. Benyounis, "Surface hardening of commercially pure titanium by laser nitriding: Response surface analysis," *Advances in engineering software*, vol. 41, pp. 674-679, 2010.

[17] S. S. Da Rocha, G. L. Adabo, G. E. Henriques and M. A. Nobilo, "Vickers Hardness of cast commercially pure titanium and T-6Al-4V Alloy submitted to heat treatments," *Brazilian Dental Journal*, vol. 17, no. 2, pp. 126-129, 2006.

[18] K. G. Budinski and M. K. Budinski, Engineering Materials: Properties and Selection, New Jersey: Pearson , 2010.

[19] P. A. Kobryn, E. H. Moore and S. L. Semiatin, "The Effect of Laser Power and Traverse Speed on Microstructure, porosity, and build height in laser-deposited Ti-6Al-4V," *Scripta Materialia*, vol. 43, no. 4, pp. 299-305, 2000.

[20] R. M. Mahamood, E. T. Akinlabi, M. Shukla and S. Pityana, "Parameters on the Porosity of Laser deposited titanium alloy powder," in *IMECS: Proceedings of the international MultiConference of Engineers and Computer Scientists* , Hong Kong, 2014.

[21] C. G. McCracken, C. Motchenbacher and D. P. Barbis, "Review of Titanium-powder-production methods," *international journal of powder metallurgy*, vol. 46, no. 5, pp. 19-26, 2010.

ISBN: 978-988-14048-0-0
ISSN: 2078-0958 (Print); ISSN: 2078-0966 (Online)